International Journal of Biological Macromolecules 183 (2021) 2131–2141

Contents lists available at ScienceDirect

International Journal of Biological Macromolecules

journal homepage: www.elsevier.com/locate/ijbiomac

Enamel-like tissue regeneration by using biomimetic enamel matrix proteins

Zehui Fang [a,1], Mengxi Guo [a,1], Qingli Zhou [a], Quanli Li [a], Hai Ming Wong [b], Chris Ying Cao [a,*]

[a] Stomatologic Hospital & College, Anhui Medical University, Key Lab.of Oral Diseases Research of Anhui Province, Hefei, 230032, China
[b] Paediatric Dentistry and Orthodontics, Faculty of Dentistry, The University of Hong Kong, 34 Hospital Road, Hong Kong

ARTICLE INFO

Keywords:
Biomimetic regeneration
Enamel
Extracellular matrix proteins

ABSTRACT

Enamel regeneration currently -is limited by our inability to duplicate artificially its complicated and well-aligned hydroxyapatite structure. The initial formation of enamel occurs in enamel organs where the ameloblasts secret enamel extracellular matrix formed a unique gel-like microenvironment. The enamel extracellular matrix is mainly composed by amelogenin and non-amelogenin. In this study, an innovative strategy was proposed to regenerate enamel-like tissue by constructing a microenvironment using biomimetic enamel matrix proteins (biomimetic EMPs) composed of modified leucine-rich amelogenin peptide (mLRAP) and non-amelogenin analog (NAA). Impressively, the regenerated enamel in this biomimetic EMPs on etched enamel surface produced prismatic structures, and showed similar mechanical properties to natural enamel. The results of X-ray diffraction (XRD) and Fourier transform infrared spectroscopy (FTIR) showed that regenerated crystal was hydroxyapatite. Molecular dynamics simulation analysis showed the binding energy between mLRAP and NAA were electrostatic forces and Van der Walls. These results introduced a promising strategy to induce crystal growth of enamel-like hydroxyapatite for biomimetic reproduction of materials with complicated hierarchical microstructures.

1. Introduction

A fundamental part of enamel biomineralization is the complex extracellular macromolecular framework in which extracellular matrix (ECM) proteins regulate mineral nucleation and growth to create enamel with outstanding mechanical properties [1]. Biomineralization is a detailed biological-physical-chemical multifactorial process in which organic substrates interact with inorganic crystals under the regulation of genetically programmed cells. An enamel prism is a very complex crystalline and molecular structure to which at least three ameloblasts (of the enamel organ) must contribute together. Hydroxyapatite (HAP) is generic formula and HAP of enamel prism is a specific crystalline pattern of HAP. A mature enamel is the hardest bioceramic in a vertebrate body and covers and protects dentin in teeth, mainly composed of 95% highly organized nanorod-like hydroxyapatite (HAP) crystals, 4% water, and less than 1% organic macromolecules that are mostly concentrated at the periphery of the prism bundles [2–4]. The hardness and toughness of a tooth enamel are mostly attributed to crystals that show some special structures: elongated in the *c*-axial direction, high aspect ratios, and bundled together to form enamel prisms [5]. However, a tooth enamel is the first to suffer defects because it lies on the outermost tooth crown layer. Tooth caries, dental trauma, and abrasion can cause dentin hypersensitivity, toothache, and pulp infection, which cause pain [6]. A fully mature enamel is acellular and therefore cannot resorb or regenerate itself. Mainly for geometric reasons, the enamel prisms have S course, proceeding from the dentin to the dental crown surface. Until now, no applicable repair for clinical development has been achieved because the complicated and well-aligned hierarchical microstructure of natural enamel cannot be duplicated at large scale artificially.

During enamel formation (amelogenesis), ameloblasts deposit enamel matrices onto predentin at the advanced bell stage. The ameloblasts undergo apoptosis after enamel is formed [7]. One of the widespread methods for restoring enamel defects is applying filling materials with compositions and structures that differ from those of enamel, such as alloys, composite resins, and ceramics [5,8]. Thus, secondary caries and polymerization shrinkage at the bonding interfaces with natural tissues frequently develop over time [9–11]. Accordingly,

* Corresponding author.
E-mail address: caoying0713@gmail.com (C.Y. Cao).
[1] These authors contributed equally.

https://doi.org/10.1016/j.ijbiomac.2021.06.028
Received 23 February 2021; Received in revised form 4 June 2021; Accepted 4 June 2021
Available online 7 June 2021

developing effective means for regenerating defective enamel is necessary. Various clinical products, such as fluoride protection paint, fluoride toothpaste, and CPP-ACP paste, have been used to hinder the development of early enamel caries and regenerate enamel. However, regenerated crystals have irregular shapes and arrangements [12,13] and cannot withstand the daily functional activities of teeth. Therefore, the biomimetic remineralization of the enamel has become a focus of research. Known methods for biomimetic remineralization include the formation of N-(2-hydroxyethyl)ethylenediamine-N,N′,N′-triacetic acid-Ca (HEDTA-Ca) as a calcium ion reservoir that promotes enamel regeneration [14], stabilization of amorphous calcium phosphate (ACP) nano-precursors by peptides [15–18], formation of enamel-like HAP nanorods using amelogenin and its analogs [19–22], formation of ACP nano-precursors using glutamic acid [23] or Polyacrylic acid [24], and shape regulation and orientation of growing enamel crystals using Leucine-Rich Amelogenin Peptide (LRAP) [25]. However, these methods are accomplished in aqueous solution, in which the microenvironment of biomimetic remineralization are very different from the enamel matrix where the enamel formation.

During enamel development, enamel matrix proteins (EMPs) play a critical role in the regulation of mineralization and crystal organization [26]. Amelogenin is the most abundant protein in a forming enamel, constituting more than 90% of ECM [27,28]. LRAP is a naturally occurring splice variant that preserves the charged N- and C-termini of a full-length amelogenin, which are crucial to interactions with HAP. The importance of LRAP for enamel crystal formation has been confirmed in mouse models [29]. Recent studies on LRAP as an amelogenin isoform indicated that LRAP was capable of promoting the remineralization of enamel surface lesions effectively the same as full-length amelogenin [25,30–32]. Therefore, LRAP can be used as an ideal substitute for amelogenin [33]. Although amelogenin plays an indispensable role in enamel development, a small amount of mineralized enamel still exists in amelogenin-deficient mouse teeth. This finding suggests that amelogenin is not necessary to initiate mineralization, and non-amelogenin enamel proteins may be involved [27], such as enamelin and ameloblastin, which are critical to normal enamel formation [34]. Recent work has already demonstrated that amelogenin alone is a weak promoter of nucleation, but addition of enamelin enhanced nucleation rates in a highly nonlinear [35]. The non-amelogenin may play a vital role in promoting mineralization in the enamel developing process.

Amelogenin and non-amelogenin are natural proteins that are difficult to extract and purify, as it can easily denature and are subject to potential contamination. However, polypeptide biomaterials have simple structures and good stability, are easy to disinfect and store, can simulate the functions of natural proteins, and can overcome the problems in the application of natural proteins. In the present study, we used synthetic peptides to mimic the function of EMPs to regenerate enamel. In the interaction between amelogenin and non-amelogenin proteins, the key component of amelogenin is the 3-tyrosine peptide domain "PYPSYGYEPMGGW" at its N-terminal [36]. We grafted this domain to the N-terminal of LRAP to afford the modified LRAP (mLRAP) the ability to interact with non-amelogenin. Non-amelogenin protein is an acidic and hydrophilic molecule with glycosylation and phosphorylation sites. It has showed that non-amelogenins interact with amelogenins through the *N*-acetyl-D-glucosamine (GlcNAc) [37]. Researchers found that the GlcNAc-mimicking peptides "SFGSGFGGGY" can bind to amelogenin [36] through the "PYPSYGYEPMGGW" domain of the amelogenin [38]. Therefore, a non-amelogenin analog (NAA) was designed by connecting the amelogenin-interaction domain of GlcNAc-mimicking peptides to a small acidic hydrophilic peptide containing two phosphorylated serine molecules. The N-terminal of this NAA is glycosylated. The aim of the present study is to regenerate enamel-like tissue to repair enamel loss by constructing a microenvironment using biomimetic EMPs composed of mLRAP and NAA.

2. Materials and methods

2.1. Design and synthesis of the mLRAP and NAA

The mLRAP with an amino acid sequence of "PYPSYGYEPMGGW-MPLPPHPGH PGYINFSYEVLTPLKWYQNMIRHPSLLPDLPLEAWPATDK TKREEVD" was produced by connecting the non-amelogenin interaction domain of amelogenin "PYPSYGYEPMGGW" to LRAP. An amelogenin-interaction domain of non-amelogenin "SFGSGFGGGY" was connected to a small acidic hydrophilic peptide containing two phosphorylated serine "ES(*p*)NES(p)" molecules, which can induce the nucleation and growth of apatite crystals. An NAA with an amino acid sequence of "GlcNAc-SFGSGFGGGY-ES(*p*)NES(p)" was produced by the acetyl amino glycosylation of the N-terminal (*N*-acetylglucosamine, GlcNAc) of "SFGSGFGGGY-ES(*p*)NES(p)." The mLRAP and NAA were synthesized by standard solid-phase peptide synthesis and purified and characterized by high-performance liquid chromatography and mass spectrometry.

2.2. Molecular docking and molecular dynamics simulation analysis of the molecular interaction between mLRAP and NAA

The interaction mechanism was explored with MD simulation, which offers computer simulation for the analysis of molecular structures and energy changes in interactions in reaction systems, facilitating a fundamental understanding of the interaction mechanisms. The secondary structures of the mLRAP and NAA were constructed according to the amino acid sequences of the two peptides, which were simulated by ITASSER online service. The structure of *N*-acetylglucosamine in the NAA was established and optimized by the B3LYP method with 6–31G* basis set in Gaussian 09 package. The parameters of mLRAP and NAA were transformed into the general AMBER force field form by the antechamber tool. The charges of mLRAP and NAA were obtained by the RESP method, and the model of interaction of mLRAP and NAA was produced by the docking program HADDOCK. Molecular dynamics simulation time for mLRAP and NAA was set to 50 ns, and all calculations were conducted using the GROMACS 5.0.4 package [39]. When the interaction reached equilibrium, the interaction mechanism of mLRAP and NAA was analyzed. Binding energy was used in the analysis of the interaction of mLRAP and NAA.

2.3. Transmission electron microscopy analysis of the biomimetic mineralization property of mLRAP and NAA

The mLRAP with and without NAA at a total concentration of 3 mg/mL was dissolved in deionized water. The mass ratio between NAA and mLRAP was 1:9 in the mLRAP/NAA solution. After 12 h, the mLRAP/NAA solution was assembled by mixing with 5 μL 1 M calcium chloride at 37 °C. After 12 h, the mLRAP/NAA and the mLRAP solution were dropped on carbon-coated copper grids (230 mesh) and dried in air. Afterward, the copper grids were immersed in a solution containing calcium and phosphorus. After 24 h, the grids were washed with distilled water three times for the complete removal of soluble salts. Transmission electron microscopy (TEM) analysis was conducted at an accelerating voltage of 80 kV.

2.4. Cytocompatibility of the artificial ECM

Bone mesenchymal stem cells (BMSCs) were used in evaluating the cytocompatibility of the artificial ECM. The BMSCs were cultured in DMEM supplemented with 10% fetal bovine serum (Biological Industries, Israel) and 1% penicillin/streptomycin solution (Thermo Fisher Scientific) at 37 °C in a 5% CO_2 incubator. The mLRAP/NAA was cross-linked on the etched enamel surface and dried in a sterile environment at

room temperature. The control group was the sterilized etched enamel slice. Enamel slices were placed in 12-well plates, and the BMSCs were then seeded into the wells at a total density of 1×10^4 cells and incubated for 1, 3, 5, and 7 days. Cell proliferation response was evaluated with a Cell Counting Kit-8 assay (CCK-8, Dojindo Laboratories Inc., Kumamoto, Japan). At a designated time point, the slices were washed with PBS and then incubated in 1000 μL of DMEM supplemented with a 100 μL of CCK-8 reagent. After 4 h incubation at 37 °C, the supernatants were transferred to a new 96-well plate, and the absorbance was measured using an automated microplate reader (MQX200, BioTek, USA) at 450 nm. Optical density absorbance values were analyzed by GraphPad Prism software and compared by *t*-test. The enamel slices were removed, and BMSCs in the 12-well plates were fixed with 2.5% glutaraldehyde for 24 h and Giemsa stain for 15 min. The morphology of the BMSCs was observed with a light microscope.

2.5. Enamel-like tissue regeneration by using biomimetic EMPs

All the following experimental methods and protocols on the use of human tissue samples were carried out in accordance with relevant guidelines and regulations. Extracted sound human third molars which were obtained with patients' consent provided in hardcopy forms. The teeth were sterilized with 3% sodium hypochlorite and rinsed with PBS. Enamel slices of 2 mm in thickness were prepared perpendicular to the longitudinal axis of each tooth by using a low-speed diamond saw (SYJ-160 Low Speed Diamond Saw, Kejing, China). The slices were polished with 400, 800, 1200, 1500, and 2000 grit silicon carbide papers under running water and then ultrasonically cleaned with acetone, ethanol, and deionized water successively. The slices were stored in deionized water at 4 °C before treatment.

Enamel slices were etched with 37% phosphoric acid for 30 s, rinsed with deionized water, and placed into polyethylene tubes. The experiment was divided into four groups. In the experimental group, half of the enamel surface was covered with acid-resistant and hydrophobic nail varnish for comparison, and the nail varnish was removed in acetone to expose the control enamel surface after the experiment. The remaining area was covered with mLRAP and NAA and cross-linked with 1-(3-Dimethylaminopropyl)-3-ethylcarbodiimide hydrochloride and N-Hydroxy succinimide (EDC/NHS). The concentration of mLRAP was set of 3 mg/mL and NAA/mLRAP mass ratio of 1:9. After the mLRAP/NAA were dried in air at room temperature, the tooth slices were immersed in simulated body fluid. The enamel surfaces covered with mLRAP and NAA, respectively, were served as two control groups. In the blank control group, a gel was prepared by mixing gelatin (8.6 g), glycerine (8.2 g), and H_2O (11.8 g). This gelatin was used to mimic the gel-like environment of ECM [40]. After gelatification, the polyethylene tubes were filled with simulated body fluid.

The polyethylene tubes were sealed and incubated in a 37 °C water bath. After 24 h, the slices were removed and cleaned ultrasonically in deionized water before SEM evaluation. XRD was used in detecting the compositions and structures of the surface layers of the enamel slices at 2θ range of 5°–60°. The results were processed in Origin 8.0 (OriginLab, USA) and then compared with the standard diffraction peak cards of HAP (JCPDS No. 09-0432). The surface groups of the enamel slices were detected by FTIR. The mechanical properties of the regenerated enamel were evaluated by microhardness test (MHV-2000Z micro Vickers, Caikon, China). Sixteen indentations were made on the surfaces of the regenerated enamel, natural enamel, and etched enamel of each slice. The time for loading was 15 s, and 10 g (0.098 N) loading force was applied. The data were processed and analyzed statistically by SPSS (SPSS Statistics 19, IBM) with one-way ANOVA. Any difference was deemed statistically significant when $P < 0.05$. SEM was used in the evaluation of the residual indent impressions on enamel surfaces.

3. Results

3.1. Design and synthesis of mLRAP and NAA

The purity of the obtained mLRAP and NAA was beyond 98% (Fig. 1A1, B1). The mass spectra of the purified mLRAP and NAA showed peaks corresponding to the molecular weights of 8023 and 1843 Da, which were close to the theoretical molecular weight (Fig. 1A2, B2). mLRAP and NAA self-assemble to form nanosphere structures that further assemble to form a supramolecular fibrous framework (Fig. 2A). At a high magnification, the fibers appeared interconnected with one another, and the fibers were composed of nanospheres (Fig. 2B). The interlinking between the nanospheres resulted in the formation of beaded chains composed of the fibers.

3.2. Biomimetic mineralization property of mLRAP and NAA

After being immersed in calcium solution, the mLRAP can spontaneously self-assembled into a nanosphere structure. TEM micrographs revealed that the linear arrangement of mLRAP was the result of the association of nanospheres (Fig. 3A). At 3 mg/mL concentration, the diameter of mLRAP nanospheres was ~200 nm. When NAA was added into the mLRAP solution, the diameter of the nanospheres (~50 nm) decreased due to the interaction and co-assembly between mLRAP and NAA (Fig. 3B). The mLRAP and NAA co-assemble into nanospheres and interlink together to form a beaded chain. This result corresponded well to the results of SEM (Fig. 2). After the self-assembled mLRAP/NAA was immersed in a solution containing calcium and phosphorus for 24 h, nanocrystals precipitated along the chain of mLRAP/NAA. This result indicated that the mLRAP/NAA can attract calcium and phosphorus ions. The electron diffraction pattern suggested that the precipitates were comparable to ACP (Fig. 3C).

3.3. Molecular dynamics (MD) simulation and molecular docking energy analyses

The MD simulation analysis also verified the interaction between mLRAP and NAA (Fig. 4). The molecule secondary structure conformations analysis of aminopeptidase sequence obtained by the I-TASSER method showed that mLRAP was helical and had extended strands and random coil. The structure of mLRAP and NAA was modeled using I-TASSER, where the C-scores of mLRAP and NAA were −3.81 and −1.48, respectively, indicating that the models had high confidence. Fig. 4A and B show the unique molecular conformations of mLRAP and NAA, respectively. The two oligopeptides interacted primarily by the designed amino acid sequences in the head region (Fig. 4C). Fig. 4D shows the binding energy of mLRAP and NAA in the interaction system. The black and red curves represented the evaluation of electrostatic forces and Van der Walls, respectively. The two curves dropped at onset and reached equilibrium, demonstrating the existence of electrostatic force and Van der Walls in the interaction system. Electrostatic interactions were the primary driving forces in the interaction system. Fig. 4E and F show the binding energy of different amino acid residues in mLRAP and NAA, respectively. The amino acid residues PRO1, TYR5, and GLU8 in mLRAP showed strong electrostatic interactions with the amino acid residues GLY3, SER4, GLY5, PHE6, GLY7, GLY9, SER12, and ASN13 in NAA. The amino acid residues TYR7, PRO9, and MET10 in mLRAP showed strong Van der Walls interactions with the acetyl amino glycosylation of N-terminal NAG1 and amino acid residue GLY8 in NAA. The acetyl amino glycosylation of the N-terminal of NAA promoted electrostatic and Van der Walls interaction with mLRAP. Although tri-tyrosine motif (PYPSYGYEPMGGW) is present in the mLRAP N-terminal region, TYR5 shows stronger electrostatic interactions with amino acid residues in NAA. Electrostatic interactions are the primary driving force; the acetyl

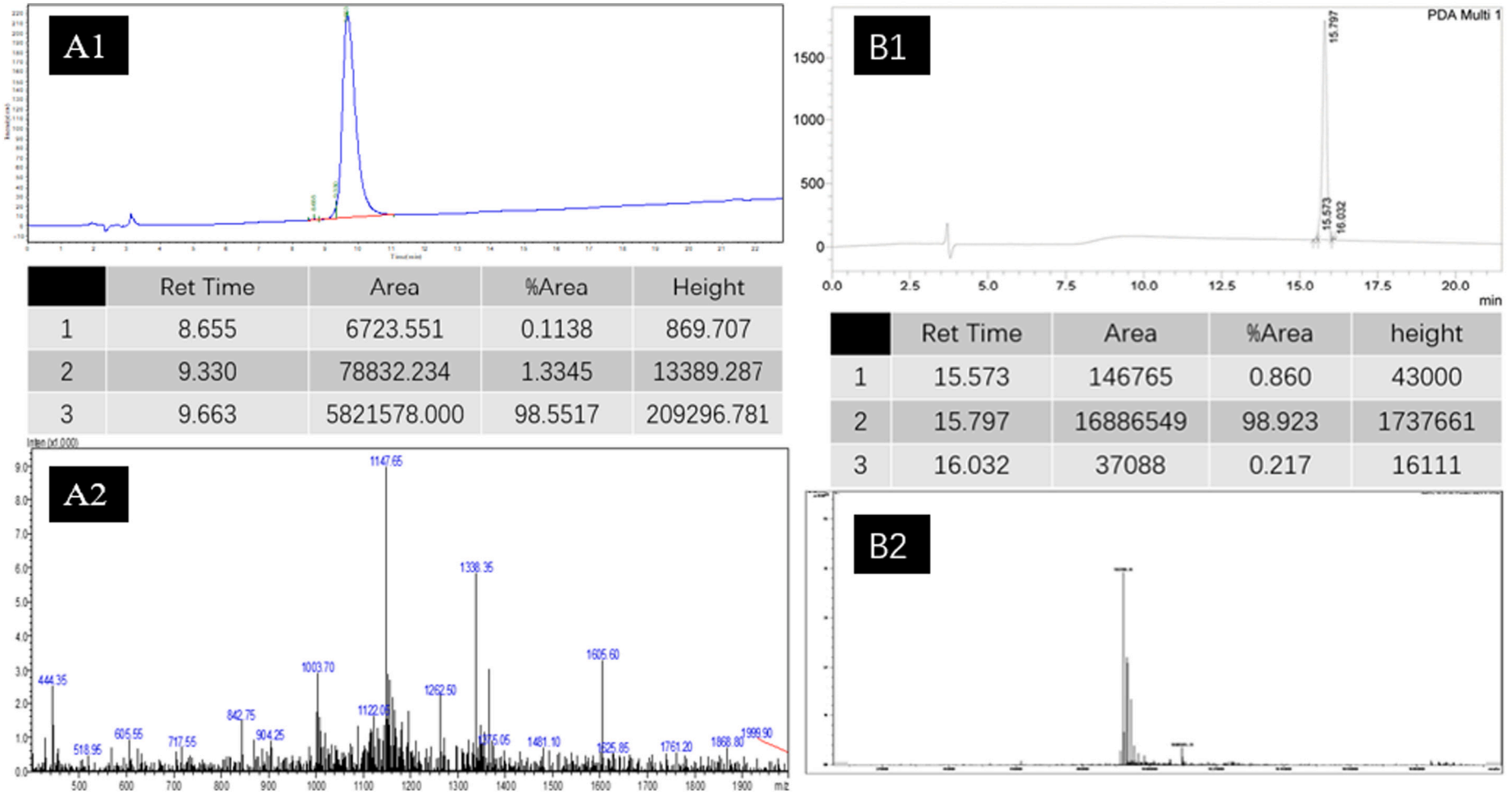

	Ret Time	Area	%Area	Height
1	8.655	6723.551	0.1138	869.707
2	9.330	78832.234	1.3345	13389.287
3	9.663	5821578.000	98.5517	209296.781

	Ret Time	Area	%Area	height
1	15.573	146765	0.860	43000
2	15.797	16886549	98.923	1737661
3	16.032	37088	0.217	16111

Fig. 1. HPLC (A1, B1) and Mass spectrometry (A2, B2) results of the synthetic mLRAP (A) and NAA (B).

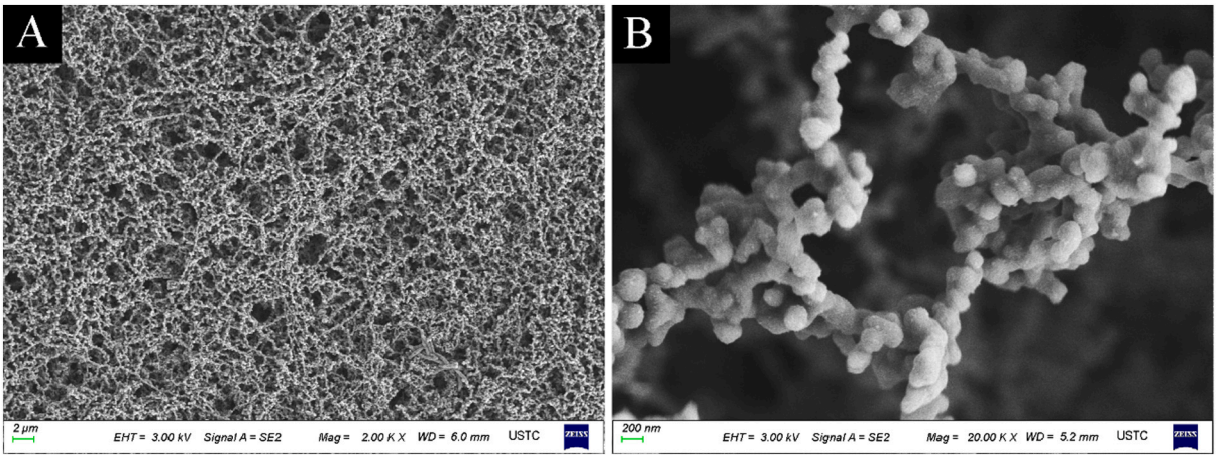

Fig. 2. (A) SEM micrographs of the self-assembly fibrous framework of mLRAP and NAA. (B) High magnification of (A).

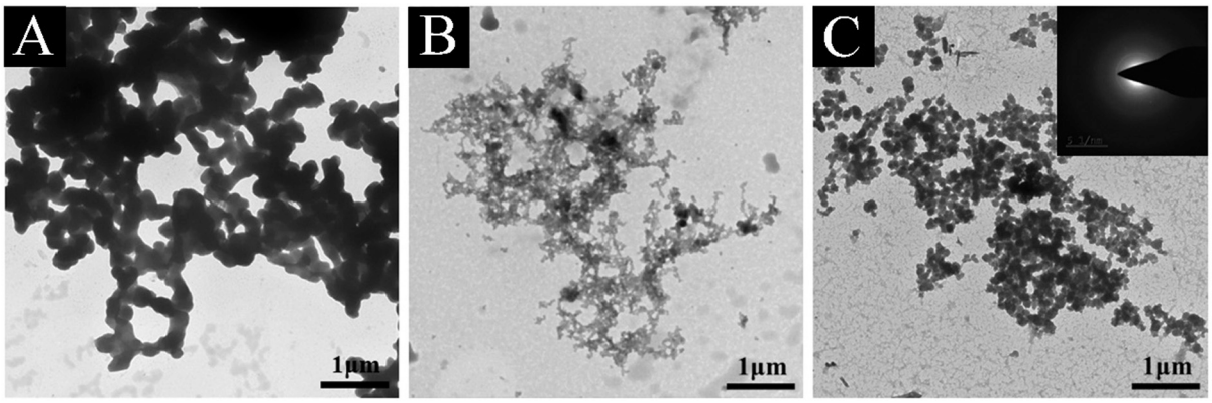

Fig. 3. TEM micrographs of self-assembled mLRAP and NAA. (A) The mLRAP. (B) The mLRAP/NAA. (C) The mLRAP/NAA was mineralized for 24 h.

amino glycosylation of N-terminal of NAA contributes to electrostatic and Van der Walls interaction with mLRAP.

3.4. Cytocompatibility of the mLRAP and NAA

The proliferation behavior of BMSCs at 1, 3, 5, and 7 days in the mLRAP/NAA group was similar to that in control group, and no significant absorbance difference was observed during the cell culturing span ($P > 0.05$; Fig.5A). The light microscopy micrographs of BMSCs in the 12-well plates in all groups revealed healthy cell morphology. BMSCs proliferation was not significantly different between the mLRAP/NAA and control groups (Fig. 5B, C). This result coincided with the results of the optical density.

3.5. SEM examination of the regenerated crystals on etched enamel surface

In the blank control group, no crystals were found on the etched enamel surface after 24 h (Fig. 6A). There were also no obvious crystals formation in the mLRAP group (Fig. 6B) and NAA group (Fig. 6C). In the experimental group, the regenerated enamel had the similar morphological texture as natural acid-etched enamel (Fig. 6D, G). The dissolution of prism cores and boundary regions was observed on the etched enamel surface. The prisms were approximately 5 μm in diameter with interprismatic less-ordered enamel in between (Fig. 6E). After the enamel surfaces were treated with biomimetic enamel matrix proteins for 24 h, the crystals precipitated on the etched enamel surface formed a prismatic and interprismatic structures with a mean diameter of approximately 5 μm, which had a similar appearance to a natural enamel microstructure. The regenerated crystals arranged and grew in the correct conformation and produced an evenly prismatic and interprismatic enamel surface (Fig. 6F). The parallel bundles of numerous needle-like crystals were fused together and densely packed on the etched enamel surface, resulting in an enamel prism-like structure. The diameters of the crystals formed were similar to those of natural enamel crystals. The transition zone between the etched enamel to the regenerated enamel (protected by nail varnish during the regeneration) demonstrates successful epitaxial growth (Fig. 6H). The cross-sectional micrograph showed that the newly regenerated layer was tightly conjoined to its underlying natural enamel, and the long axes of the newly regenerated crystals corresponded to the crystallographic *c*-axis of the underlying HAP crystals. Moreover, the microstructures of the regenerated layer were morphologically similar to those of its underlying natural enamel. The thickness of the regenerated enamel layer was approximately 2 μm, with well-organized and uniform characteristics. No evident boundary was found at the interface (Fig. 6I).

3.6. XRD and FTIR characterization of the regenerated crystals

The mineral phase of the regenerated enamel layer was monitored through XRD (Fig. 7A). All the diffraction peaks corresponded well to the peaks for hexagonal phase HAP (JCPDS#09-0432) crystals, implying an identically organized crystallographic structure at the macroscopic level. The sharp and intense 002 and 004 peaks in line c indicated that the regenerated crystals were well crystallized and oriented parallel along the *c*-axis direction; this result was consistent with the

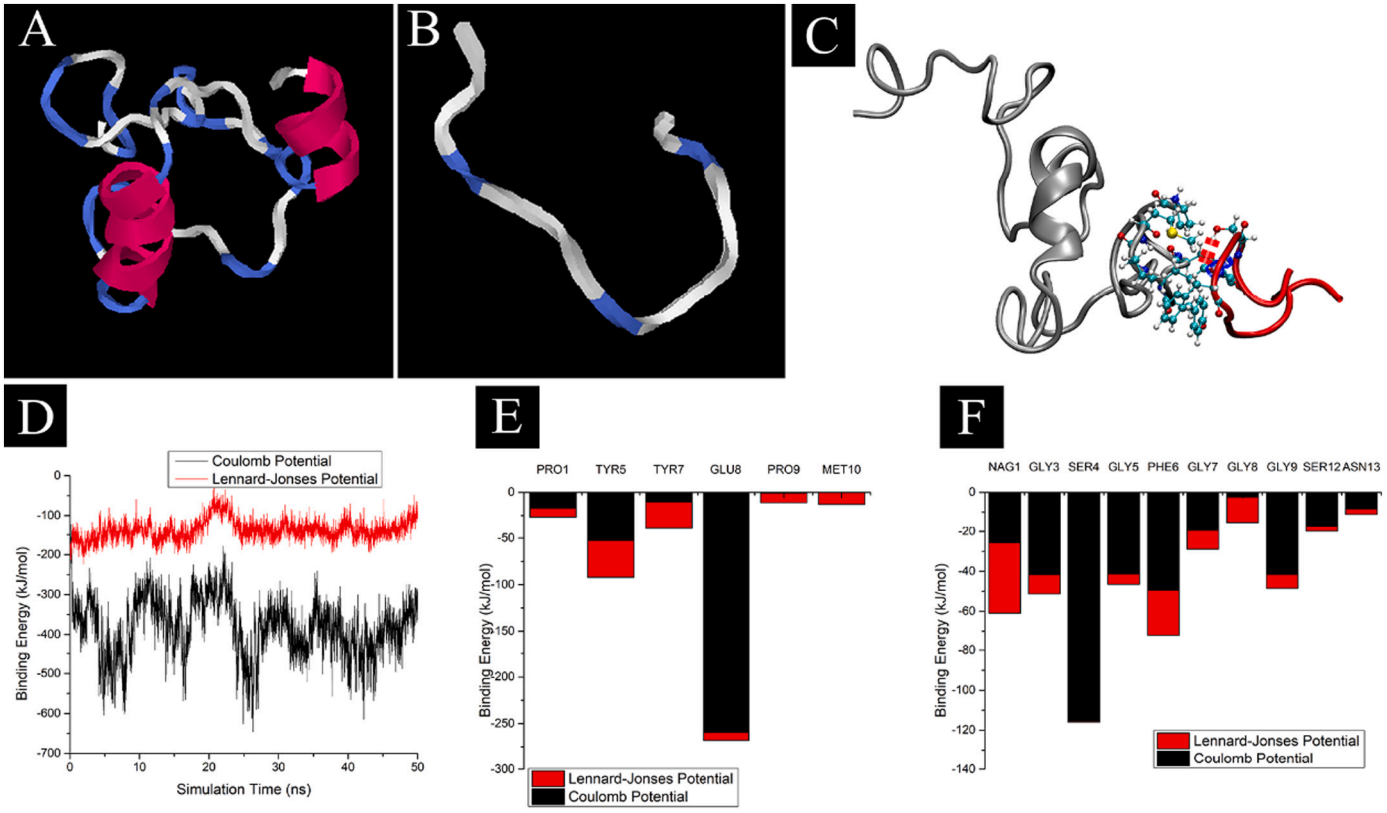

Fig. 4. MD simulation analysis and Molecular Docking Energy Analysis. (A) The secondary structure of mLRAP. (B) The secondary structure of NAA. (C) The simulation of interaction between mLRAP and NAA. (D) Binding energy between mLRAP and NAA. (E) Binding energy between amino acid residues of mLRAP and NAA. (F) Binding energy between mLRAP and amino acid residues of NAA.

observations in the SEM images (Fig. 6). The unsplit diffraction peak at approximately 32° in line c indicated the poor crystallinity of the newly formed HAP crystals on the enamel surface The FTIR spectra confirmed the formation of a typical HAP structure (Fig. 7B). The split PO_4 $\nu 3$ band (997–1124 cm^{-1}) and the split PO_4 $\nu 4$ band (600 and 554 cm^{-1}) indicated the presence of the phosphate groups in the regenerated layer on the etched enamel surface.

3.7. Mechanical properties of the regenerated crystals

Fig. 8A illustrates the calculated microhardness of the natural, regenerated, and etched enamel. The natural enamel had optimal mechanical performance characteristics, with a 280.80 ± 37.20 HV (mean ± SD). The mechanical properties of the enamel were weakened by phosphoric acid etching, with a 184.42 ± 34.20 HV (mean ± SD). After 24 h incubation, the mean microhardness of the enamel was increased to 261.54 ± 24.61 HV (regenerated enamel). No significant differences were observed in microhardness between the regenerated and natural enamel. Fig. 8B shows a SEM image of the regenerated enamel surface with 16 indentations. The indentation impressions formed a rectangular pyramid, and no cracks were found around the indentations. The impression area on the surface of the regenerated enamel (Fig. 8E) was similar to that on the untreated enamel (Fig. 8D), and both were smaller than the etched enamel (Fig. 8C).

4. Discussion

Dental enamel formation is an example of protein matrix-mediated biomineralization [41]. EMPs play vital roles in the regulation of mineralization and crystal organization during enamel development. EMPs predominantly comprise amelogenin, which constitutes 90%–95% of ECMs. Meanwhile, 5%–10% are non-amelogenin proteins [4]. The nonclassical crystallization pathway theory suggests that amelogenin interacts with noncrystalline calcium phosphate to form, stabilize and assemble intermediate prenucleation clusters that further transform into organized apatite crystals [42]. Amelogenin proteins form an insoluble macromolecular framework that acts as a key mediator in controlling biomineralization. The N-terminal (including the phosphorylation site) and C-terminal (including the hydrophilic domain) domains of a full-length amelogenin play important roles in proper enamel mineral formation [43]. The N-terminal is responsible for amelogenin self-assembly into “nanospheres” and the formation of chain-like structures. The C-terminal is essential for guiding the generation of parallel arrays of apatite crystals in vitro [44]. The tri-tyrosine motif (PYPSYGYEPMGGW) in the amelogenin N-terminal region is involved in amelogenin-cell or amelogenin-nonamelogenin interactions. LRAP is an alternative splicing product of the amelogenin gene expressed throughout enamel development. Porcine LRAP comprises 56 amino acids: the 33 N-terminal and 23 C-terminal amino acids of a full-length amelogenin [45]. LRAP shares certain properties with full-length amelogenin, such as forming nanospheres and interacting with HAP through its C-terminus and N-terminus [33,46]. These EMPs control the initiation, pattern, orientation, and organization of enamel crystals in a cooperative manner and are then gradually degraded and removed during enamel maturation [34]. In addition to amelogenin, small amounts of non-amelogenin proteins, such as enamelin and ameloblastin, are critical to normal enamel formation. Another potential target for amelogenin is the least abundant acidic phosphorylated glycoprotein enamelin. The interactions between amelogenin and enamelin play vital roles in controlling enamel crystal formation [34]. Adding enamelin to an amelogenin “gel-like matrix” results in an evident increase in the aspect ratios of octacalcium phosphate crystals. Moreover, the presence of enamelin in the amelogenin matrix enhances the stability of the transient ACP phase through the co-assembling of

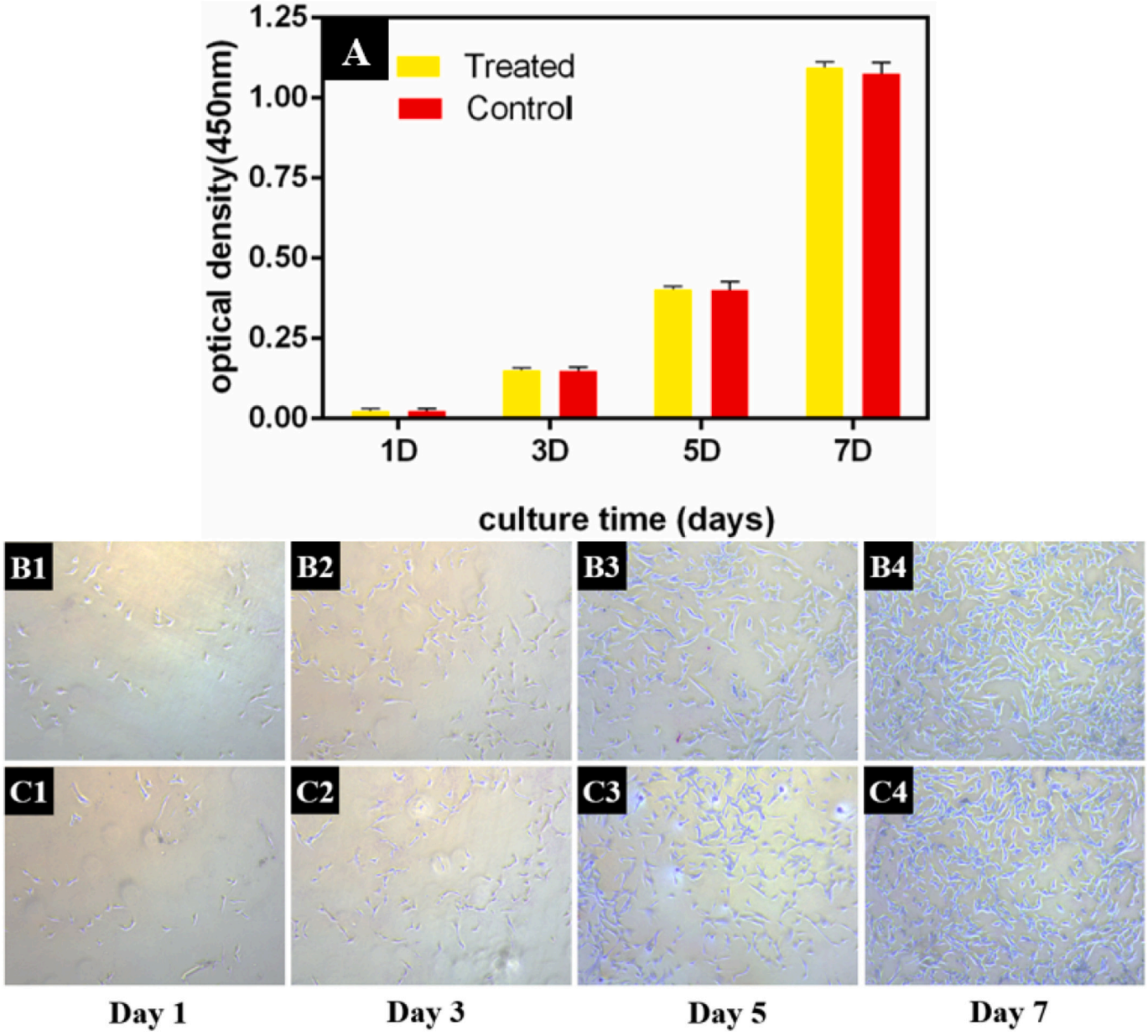

Fig. 5. Cytocompatibility evaluation of BMSCs in mLRAP/NAA group and control group. (A) Proliferation of BMSCs in mLRAP/NAA group and control group for 1, 3, 5, and 7 days by the CCK-8 assays. No difference was detected between all groups ($P > 0.05$). (B) Light microscope micrographs of BMSCs in mLRAP/NAA group. (C) Light microscope micrographs of BMSCs in control group. (Magnification 50×).

enamelin and amelogenin [47]. Enamelin has glycosylation and phosphorylation sites; these structural domains are important functional domains interacting with apatite crystals and acting as crystal nucleator of enamel apatite [48]. Through a domain of "SFGSGFGGGY" and the acetyl amino glycosylation of N-terminal (*N*-acetylglucosamine, NAG), non-amelogenin interacts with the domain "PYPSYGYEPMGGW" of amelogenin [36]. Therefore, in the present study, LRAP was modified by grafting the tri-tyrosine motif (PYPSYGYEPMGGW) in its N-terminal region to mimic the function of amelogenin and the interaction between amelogenin and non-amelogenin. Many acidic glycoproteins not only act as strong inhibitors of crystal nucleation and growth in solution but also can serve as effective nucleators once they have been adsorbed onto the surfaces and adopted defined structures. The previous study showed that a single phosphate group on serine-16 is involved in amelogenin–calcium phosphate interactions and contributes to the stabilization of ACP precursors [49]. A small acidic hydrophilic peptide containing two phosphorylated serine "ES(*p*)NES(p)" grafted the amelogenin-interaction domain of GlcNAc-mimicking peptides "SFGSGFGGGY" and glycosylated its N-terminal to mimic the function of non-amelogenin proteins and the interaction between amelogenin and non-amelogenin proteins. mLRAP and NAA control the process of crystal nucleation, which is mediated through molecular interactions, such as protein–protein (mLRAP self-assembly and mLRAP-NAA interactions) and mLRAP/NAA-mineral interactions. In the present study, when NAA was added into the mLRAP solution, the diameter of the nanospheres decreased. The mLRAP and NAA co-assemble into nanospheres and interlink together to form a beaded chain, demonstrating the interaction and co-assembly of mLRAP and NAA. This phenomenon is similar to the ability of non-amelogenin in promoting the amelogenin to form a three-dimensional structure in the process of natural enamel formation [37]. The interaction between amelogenins and non-amelogenins have influence in developing HAP crystals in natural enamel formation. Non-

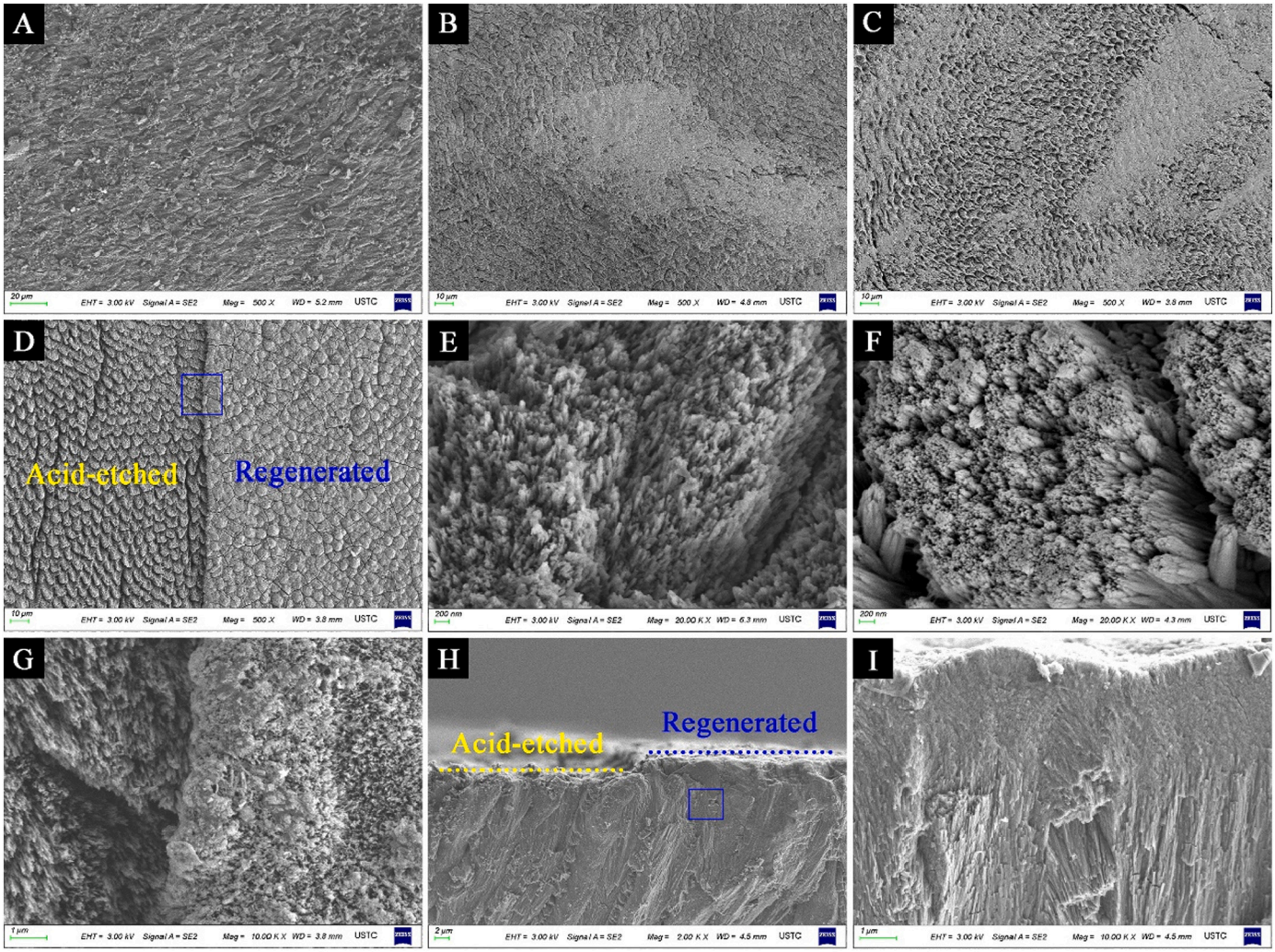

Fig. 6. SEM micrographs of acid-etched enamel and the regenerated enamel after incubated in the artificial ECM for 24 h. (A) SEM micrograph of blank control group. (B) SEM micrograph of mLRAP group (C) SEM micrograph of NAA group (D) SEM micrograph showing both acid-etched enamel and regenerated enamel. (E) Magnified micrograph of the acid-etched enamel. (F) Magnified micrograph of the regenerated enamel. (G) Magnified micrograph of the blue rectangular area in panel D. (H) Cross-sectional view from acid-etched enamel to the regenerated enamel. (I) Magnified micrograph of the blue rectangular area in panel H. (For interpretation of the references to colour in this figure legend, the reader is referred to the web version of this article.)

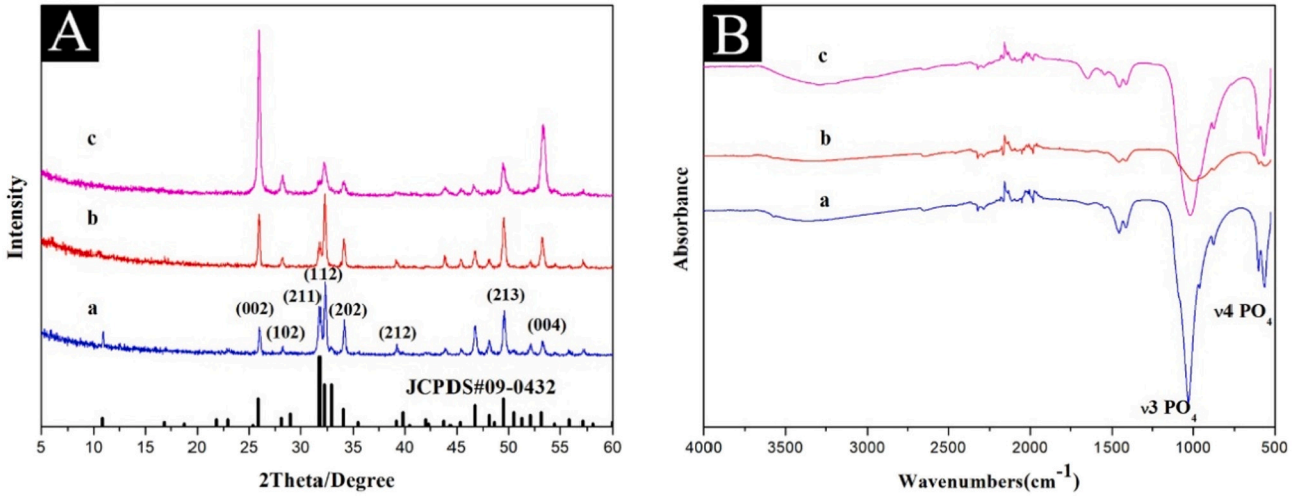

Fig. 7. XRD (A) and FTIR (B) spectra of the regenerated layer on the enamel surface. (a) Acid-etched enamel. (b) Natural enamel. (c) The regenerated enamel layer after incubated in the artificial ECM for 24 h.

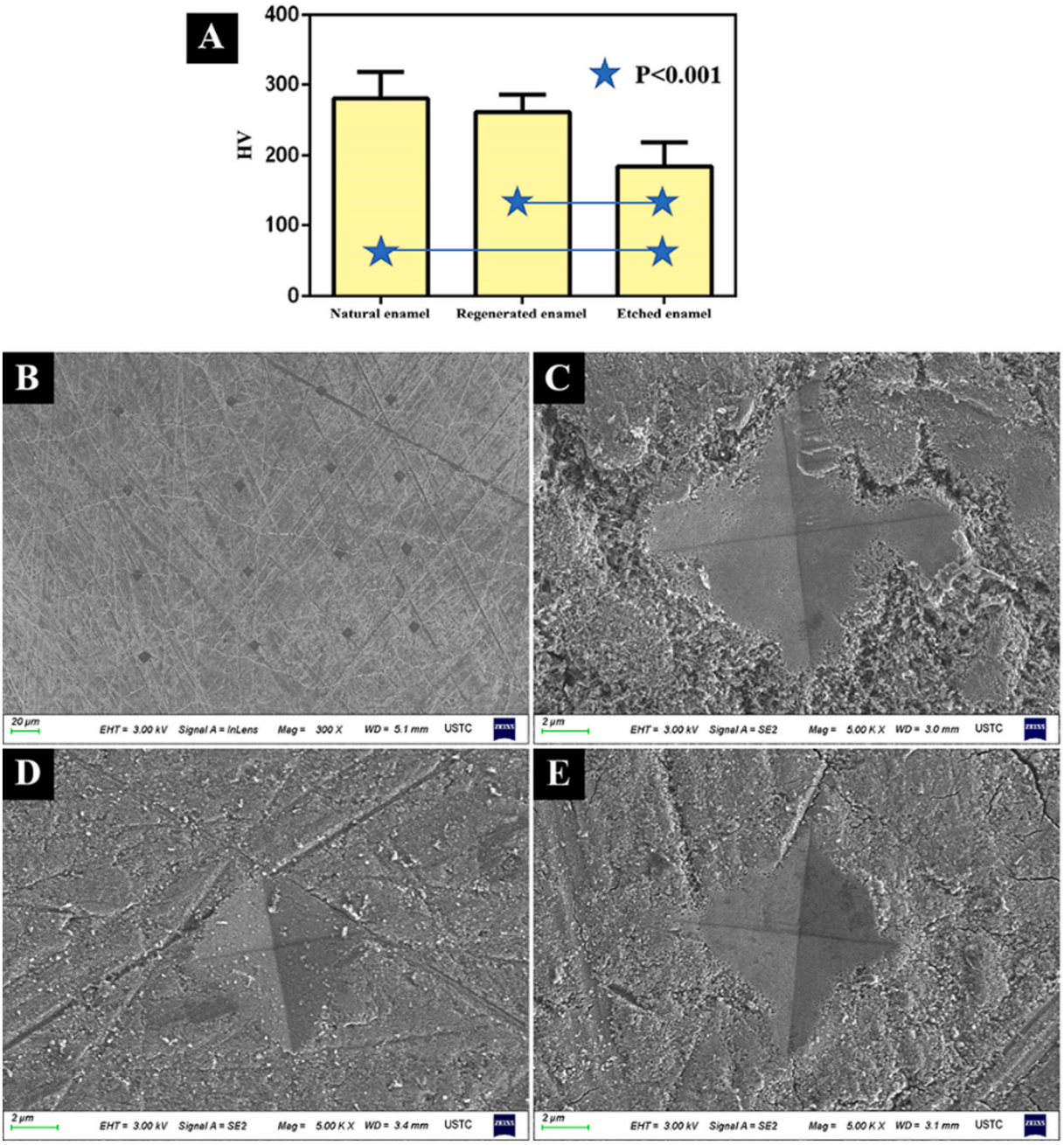

Fig. 8. The mechanical property of the enamel samples. (A) Calculated microhardness of the enamel samples. (B) SEM image of the regenerated enamel surface with indentations. (C) SEM image of the indentation impression on the etched enamel surface. (D) SEM image of the indentation impression on the natural enamel surface. (E) SEM image of the indentation impression on the regenerated enamel surface.

amelogenins have significant higher Ca^{2+}-binding constant than amelogenins [50]. The GlcNAc residual and two phosphorylated serine in NAA absorb calcium ion and promote the HAP crystals formation. When NAA binding to mLRAP, the mLRAP/NAA may absorb more Ca^{2+} than mLRAP alone and promote crystal nucleation. In vivo, the amelogenin self-assembly to form nanosphere before the enamel mineralization [51,52]. Researchers has showed that the amelogenin regulate enamel formation when it self-assembly into nanospheres [53,54]. The self-assembly of amelogenin is critical for its function in enamel mineralization. Amelogenin self-assembly is the driving force for crystal organization, which believed to be a key factor in controlling the oriented and elongated growth of the hydroxyapatite crystals within enamel prisms [55].

The MD simulation analysis verified the interaction between mLRAP and NAA. Although tri-tyrosine motif (PYPSYGYEPMGGW) is present in the mLRAP N-terminal region, TYR5 shows stronger electrostatic interactions with amino acid residues in NAA. Electrostatic interactions are the primary driving force; the acetyl amino glycosylation of N-terminal of NAA contributes to electrostatic and Van der Walls interaction with mLRAP. In biomimetic mineralization, inorganic minerals are deposited by precipitates arising from secondary interactions with the surrounding environment. In our present study, the calcium and phosphate ions in the remineralization environment were regulated to form the hierarchical enamel-like structures through the dynamic processes of controlled crystal formation, organization, and growth guided by mLRAP/NAA.

Recent strategies for tooth tissue engineering have utilized a variety of scaffold materials to create bioengineered teeth, such as PGA/PLGA

[56], silk fibroin [57], collagen sponge [58], and decellularized enamel organ [59]. These reports indicate that the functional characterization of teeth expressed in ECM molecules, including the respective developmental and spatial organization of ECM molecules, may facilitate the design of effective scaffolds for tooth regeneration. ECM provides morphogenetic cues that guide proper cellular interactions during natural and bioengineered organogenesis. The natural amelogenin and non-amelogenin can deliver the signals to the cells and regulate the bioengineered mineralization. Our designed mLRAP and NAA derived from the natural amelogenin and non-amelogenin may also have the property of cell signaling. The viability and cytological changes of BMSC cells are not influenced in the acellular enamel organ alternative, and thus the cells could be excellent scaffold candidates for bioengineered tooth formation.

In our present study, a gel-like microenvironment was constructed using biomimetic EMPs composed of mLRAP and NAA which mimicking the gel-like organic matrix environment during enamel formation. This microenvironment introduced a promising strategy to induce crystal growth of enamel-like hydroxyapatite for biomimetic reproduction of materials with complicated hierarchical microstructures. Compared with the reported research models, our model is closer to the physical and chemical environment of natural enamel formation. Although the regenerated hydroxyapatite crystals were different from the natural enamel hierarchical microstructure, it is essential to develop various models mimicking the assembly steps of enamel crystals and enamel-like structure formation. This proof-of-concept study demonstrated the potential of a new biomimetic approach with the gel-like microenvironment to form a biomimetic EMPs matrix on defected enamel surface, which mimicking the ability of EMPs to induce mineralization for HAP formation.

5. Conclusion

In our present study, the biomimetic enamel matrix proteins of mLRAP and NAA was designed for the regeneration of enamel-like tissues. The regenerated enamel produced a prismatic and interprismatic structures, which are also observed in natural enamel. The present study provided an important basis for the development of enamel prism-like materials that can be used in alternative treatment in clinical dentistry, tooth tissue engineering as scaffolds, and other biomedical or industrial applications.

CRediT authorship contribution statement

Zehui Fang: Data acquisition by experimentation and characterization, Writing - original draft. **Mengxi Guo**: Characterization interpretation and drafting. **Qingli Zhou**: Data acquisition by experimentation and characterization. **Quanli Li**: Conceptualization, Writing - review & editing. **Hai Ming Wong**: Conceptualization, Writing - review & editing. **Chris Ying Cao**: Supervision, Writing - review & editing.

Declaration of competing interest

None.

Acknowledgements

This study was supported by Anhui Provincial Natural Science Foundation (2008085MH254), Key Research and Development Plan of Anhui Province (202004j07020041), and National Natural Science Foundation of China (81970983). The authors declare no potential interest in this study.

References

[1] M. Pandya, T.G.H. Diekwisch, Enamel biomimetics-fiction or future of dentistry, Int. J. Oral. Sci. 11 (2019), 8, https://doi.org/10.1038/s41368-018-0038-6.
[2] Y. Cao, W. Liu, T. Ning, M.L. Mei, Q.L. Li, E.C. Lo, C.H. Chu, A novel oligopeptide simulating dentine matrix protein 1 for biomimetic mineralization of dentine, Clin. Oral Investig. 18 (2014) 873–881, https://doi.org/10.1007/s00784-013-1035-y.
[3] X. Li, J. Wang, A. Joiner, J. Chang, The remineralisation of enamel: a review of the literature, J. Dent. 42 (Suppl. 1) (2014) S12–S20, https://doi.org/10.1016/S0300-5712(14)50003-6.
[4] Q. Ruan, J. Moradian-Oldak, Amelogenin and enamel biomimetics, J. Mater. Chem. B 3 (2015) 3112–3129, https://doi.org/10.1039/c5tb00163c.
[5] K. Tian, M. Peng, X. Ren, C. Liao, W. Fei, Regeneration of tooth-like hydroxyapatite depended on amelogenin functional section monolayer: a new approach for tooth repair, Med. Hypotheses 79 (2012) 143–146, https://doi.org/10.1016/j.mehy.2012.04.017.
[6] N.X. West, A. Joiner, Enamel mineral loss, J. Dent. 42 (Suppl. 1) (2014) S2–11, https://doi.org/10.1016/S0300-5712(14)50002-4.
[7] J.E. Nor, Tooth regeneration in operative dentistry, Oper. Dent. 31 (2006) 633–642, https://doi.org/10.2341/06-000.
[8] L. Wang, X. Guan, H. Yin, J. Moradian-Oldak, G.H. Nancollas, Mimicking the self-organized microstructure of tooth enamel, J. Phys. Chem. C Nanomater. Interfaces 112 (2008) 5892–5899, https://doi.org/10.1021/jp077105+.
[9] M.D. Weir, L.C. Chow, H.H. Xu, Remineralization of demineralized enamel via calcium phosphate nanocomposite, J. Dent. Res. 91 (2012) 979–984, https://doi.org/10.1177/0022034512458288.
[10] F.F. Demarco, M.B. Correa, M.S. Cenci, R.R. Moraes, N.J. Opdam, Longevity of posterior composite restorations: not only a matter of materials, Dent. Mater. 28 (2012) 87–101, https://doi.org/10.1016/j.dental.2011.09.003.
[11] J. Wei, J. Wang, W. Shan, X. Liu, J. Ma, C. Liu, J. Fang, S. Wei, Development of fluorapatite cement for dental enamel defects repair, J. Mater. Sci. Mater. Med. 22 (2011) 1607–1614, https://doi.org/10.1007/s10856-011-4327-2.
[12] Y. Fan, J.R. Nelson, J.R. Alvarez, J. Hagan, A. Berrier, X. Xu, Amelogenin-assisted ex vivo remineralization of human enamel: effects of supersaturation degree and fluoride concentration, Acta Biomater. 7 (2011) 2293–2302, https://doi.org/10.1016/j.actbio.2011.01.028.
[13] N. Roveri, E. Battistella, C.L. Bianchi, I. Foltran, E. Foresti, M. Iafisco, M. Lelli, A. Naldoni, B. Palazzo, L. Rimondini, Surface enamel remineralization: biomimetic apatite nanocrystals and fluoride ions different effects, J. Nanomater. 2009 (2009), 746383, https://doi.org/10.1155/2009/746383.
[14] Y. Yin, S. Yun, J. Fang, H. Chen, Chemical regeneration of human tooth enamel under near-physiological conditions, Chem. Commun. (Camb.) (2009) 5892–5894, https://doi.org/10.1039/b911407f.
[15] J. Kirkham, A. Firth, D. Vernals, N. Boden, C. Robinson, R.C. Shore, S.J. Brookes, A. Aggeli, Self-assembling peptide scaffolds promote enamel remineralization, J. Dent. Res. 86 (2007) 426–430, https://doi.org/10.1177/154405910708600507.
[16] Y. Zhou, Y. Zhou, L. Gao, C. Wu, J. Chang, Synthesis of artificial dental enamel by an elastin-like polypeptide assisted biomimetic approach, J. Mater. Chem. B 6 (2018) 844–853, https://doi.org/10.1039/c7tb02576a.
[17] M. Alkilzy, A. Tarabaih, R.M. Santamaria, C.H. Splieth, Self-assembling peptide P11-4 and fluoride for regenerating enamel, J. Dent. Res. 97 (2018) 148–154, https://doi.org/10.1177/0022034517730531.
[18] Z. Xiao, K. Que, H. Wang, R. An, Z. Chen, Z. Qiu, M. Lin, J. Song, J. Yang, D. Lu, M. Shen, B. Guan, Y. Wang, X. Deng, X. Yang, Q. Cai, J. Deng, L. Ma, X. Zhang, X. Zhang, Rapid biomimetic remineralization of the demineralized enamel surface using nano-particles of amorphous calcium phosphate guided by chimaeric peptides, Dent. Mater. 33 (2017) 1217–1228, https://doi.org/10.1016/j.dental.2017.07.015.
[19] Y. Fan, Z. Sun, J. Moradian-Oldak, Controlled remineralization of enamel in the presence of amelogenin and fluoride, Biomaterials 30 (2009) 478–483, https://doi.org/10.1016/j.biomaterials.2008.10.019.
[20] M. Iijima, J. Moradian-Oldak, Control of octacalcium phosphate and apatite crystal growth by amelogenin matrices, J. Mater. Chem. 14 (2004) 2189–2199, https://doi.org/10.1039/b401961j.
[21] D. Wu, J. Yang, J. Li, L. Chen, B. Tang, X. Chen, W. Wu, J. Li, Hydroxyapatite-anchored dendrimer for in situ remineralization of human tooth enamel, Biomaterials 34 (2013) 5036–5047, https://doi.org/10.1016/j.biomaterials.2013.03.053.
[22] M. Chen, J.J. Yang, J.Y. Li, K.N. Liang, L.B. He, Z.F. Lin, X.Y. Chen, X.K. Ren, J. S. Li, Modulated regeneration of acid-etched human tooth enamel by a functionalized dendrimer that is an analog of amelogenin, Acta Biomater. 10 (2014) 4437–4446, https://doi.org/10.1016/j.actbio.2014.05.016.
[23] L. Li, C. Mao, J. Wang, X. Xu, H. Pan, Y. Deng, X. Gu, R. Tang, Bio-inspired enamel repair via Glu-directed assembly of apatite nanoparticles: an approach to biomaterials with optimal characteristics, Adv. Mater. 23 (2011) 4695–4701, https://doi.org/10.1002/adma.201102773.
[24] H. Milly, F. Festy, T.F. Watson, I. Thompson, A. Banerjee, Enamel white spot lesions can remineralise using bio-active glass and polyacrylic acid-modified bio-active glass powders, J. Dent. 42 (2014) 158–166, https://doi.org/10.1016/j.jdent.2013.11.012.
[25] S.Y. Kwak, A. Litman, H.C. Margolis, Y. Yamakoshi, J.P. Simmer, Biomimetic enamel regeneration mediated by leucine-rich amelogenin peptide, J. Dent. Res. 96 (2017) 524–530, https://doi.org/10.1177/0022034516688659.
[26] M. Iijima, J. Moradian-Oldak, Interactions of amelogenins with octacalcium phosphate crystal faces are dose dependent, Calcif. Tissue Int. 74 (2004) 522–531, https://doi.org/10.1007/s00223-002-0011-3.

[27] C.W. Gibson, Z.A. Yuan, B. Hall, G. Longenecker, E. Chen, T. Thyagarajan, T. Sreenath, J.T. Wright, S. Decker, R. Piddington, G. Harrison, A.B. Kulkarni, Amelogenin-deficient mice display an amelogenesis imperfecta phenotype, J. Biol. Chem. 276 (2001) 31871–31875, https://doi.org/10.1074/jbc.M104624200.
[28] C. Du, G. Falini, S. Fermani, C. Abbott, J. Moradian-Oldak, Supramolecular assembly of amelogenin nanospheres into birefringent microribbons, Science 307 (2005) 1450–1454, https://doi.org/10.1126/science.1105675.
[29] R.M. Ravindranath, A. Devarajan, P. Bringas Jr., Enamel formation in vitro in mouse molar explants exposed to amelogenin polypeptides ATMP and LRAP on enamel development, Arch. Oral Biol. 52 (2007) 1161–1171, https://doi.org/10.1016/j.archoralbio.2007.06.008.
[30] G.H. Bagheri, A. Sadr, J. Espigares, I. Hariri, S. Nakashima, H. Hamba, F. Shafiei, F. Moztarzadeh, J. Tagami, Study on the influence of leucine-rich amelogenin peptide (LRAP) on the remineralization of enamel defects via micro-focus x-ray computed tomography and nanoindentation, Biomed. Mater. 10 (2015), 035007, https://doi.org/10.1088/1748-6041/10/3/035007.
[31] F. Shafiei, B.G. Hossein, M.M. Farajollahi, M. Fathollah, B. Marjan, J.K. Tahereh, Leucine-rich amelogenin peptide (LRAP) as a surface primer for biomimetic remineralization of superficial enamel defects: an in vitro study, Scanning 37 (2015) 179–185, https://doi.org/10.1002/sca.21196.
[32] K. Mukherjee, Q.C. Ruan, D. Liberman, S.N. White, J. Moradian-Oldak, Repairing human tooth enamel with leucine-rich amelogenin peptide-chitosan hydrogel, J. Mater. Res. 31 (2016) 556–563, https://doi.org/10.1557/jmr.2016.64.
[33] E. Le Norcy, S.Y. Kwak, F.B. Wiedemann-Bidlack, E. Beniash, Y. Yamakoshi, J. P. Simmer, H.C. Margolis, Leucine-rich amelogenin peptides regulate mineralization in vitro, J. Dent. Res. 90 (2011) 1091–1097, https://doi.org/10.1177/0022034511411301.
[34] J. Moradian-Oldak, Protein-mediated enamel mineralization, Front. Biosci.-Landmrk 17 (2012) 1996–2023, https://doi.org/10.2741/4034.
[35] J.H. Tao, A. Fijneman, J.Q. Wan, S. Prajapati, K. Mukherjee, A. Fernandez-Martinez, J. Moradian-Oldak, J.J. De Yoreo, Control of calcium phosphate nucleation and transformation through interactions of enamelin and amelogenin exhibits the “goldilocks effect”, Cryst. Growth Des. 18 (2018) 7391–7400, https://doi.org/10.1021/acs.cgd.8b01066.
[36] R.M. Ravindranath, W.Y. Tam, P. Nguyen, A.G. Fincham, The enamel protein amelogenin binds to the N-acetyl-D-glucosamine-mimicking peptide motif of cytokeratins, J. Biol. Chem. 275 (2000) 39654–39661, https://doi.org/10.1074/jbc.M006471200.
[37] R.M. Ravindranath, J. Moradian-Oldak, A.G. Fincham, Tyrosyl motif in amelogenins binds N-acetyl-D-glucosamine, J. Biol. Chem. 274 (1999) 2464–2471, https://doi.org/10.1074/jbc.274.4.2464.
[38] H.H. Ravindranath, L.-S. Chen, M. Zeichner-David, R. Ishima, R.M. H. Ravindranath, Interaction between the enamel matrix proteins amelogenin and ameloblastin, Biochem. Biophys. Res. Commun. 323 (2004) 1075–1083, https://doi.org/10.1016/j.bbrc.2004.08.207.
[39] H. Rakhshani, E. Dehghanian, A. Rahati, Enhanced GROMACS: toward a better numerical simulation framework, J. Mol. Model. 25 (2019), 355, https://doi.org/10.1007/s00894-019-4232-z.
[40] S. Busch, Regeneration of human tooth enamel, Angew. Chem. Int. Ed. Eng. 43 (2004) 1428–1431, https://doi.org/10.1002/anie.200352183.
[41] Z. Ling, Y. He, H. Huang, X. Xie, Q.L. Li, C.Y. Cao, Effects of oligopeptide simulating DMP-1/mineral trioxide aggregate/agarose hydrogel biomimetic mineralisation model for the treatment of dentine hypersensitivity, J. Mater. Chem. B 7 (2019) 5825–5833, https://doi.org/10.1039/c9tb01684h.
[42] X.D. Yang, L.J. Wang, Y.L. Qin, Z. Sun, Z.J. Henneman, J. Moradian-Oldak, G. H. Nancollas, How amelogenin orchestrates the organization of hierarchical elongated microstructures of apatite, J. Phys. Chem. B 114 (2010) 2293–2300, https://doi.org/10.1021/jp910219s.
[43] M.L. Paine, W. Luo, D.H. Zhu, P. Bringas Jr., M.L. Snead, Functional domains for amelogenin revealed by compound genetic defects, J. Bone Miner. Res. 18 (2003) 466–472, https://doi.org/10.1359/jbmr.2003.18.3.466.
[44] S.Y. Kwak, F.B. Wiedemann-Bidlack, E. Beniash, Y. Yamakoshi, J.P. Simmer, A. Litman, H.C. Margolis, Role of 20-kDa amelogenin (P148) phosphorylation in calcium phosphate formation in vitro, J. Biol. Chem. 284 (2009) 18972–18979, https://doi.org/10.1074/jbc.M109.020370.
[45] A.G. Fincham, J. Moradian-Oldak, Amelogenin post-translational modifications: carboxy-terminal processing and the phosphorylation of bovine and porcine “TRAP” and “LRAP” amelogenins, Biochem. Biophys. Res. Commun. 197 (1993) 248–255, https://doi.org/10.1006/bbrc.1993.2468.
[46] J.H. Tao, Y. Shin, R. Jayasinha, G.W. Buchko, S.D. Burton, A.C. Dohnalkova, Z. M. Wang, W.J. Shaw, B.J. Tarasevich, The energetic basis for hydroxyapatite mineralization by amelogenin variants provides insights into the origin of amelogenesis imperfecta, Proc. Natl. Acad. Sci. U. S. A. 116 (2019) 13867–13872, https://doi.org/10.1073/pnas.1815654116.
[47] M. Iijima, D.M. Fan, K.M. Bromley, Z. Sun, J. Moradian-Oldak, Tooth enamel proteins enamelin and amelogenin cooperate to regulate the growth morphology of octacalcium phosphate crystals, Cryst. Growth Des. 10 (2010) 4815–4822, https://doi.org/10.1021/cg100696r.
[48] N. Bouropoulos, J. Moradian-Oldak, Induction of apatite by the cooperative effect of amelogenin and the 32-kDa enamelin, J. Dent. Res. 83 (2004) 278–282, https://doi.org/10.1177/154405910408300402.
[49] F.B. Wiedemann-Bidlack, S.Y. Kwak, E. Beniash, Y. Yamakoshi, J.P. Simmer, H. C. Margolis, Effects of phosphorylation on the self-assembly of native full-length porcine amelogenin and its regulation of calcium phosphate formation in vitro, J. Struct. Biol. 173 (2011) 250–260, https://doi.org/10.1016/j.jsb.2010.11.006.
[50] T.T.Y. Yamakoshi, S. Oida, C.-C. Hu, J.P. Simmer, M. Fukae, Calcium binding of enamel proteins and their derivatives with emphasis on the calcium-binding domain of porcine sheathlin, Arch. Oral Biol. 46 (2001) 1005–1014, https://doi.org/10.1016/s0003-9969(01)00070-x.
[51] A.G. Fincham, J. Moradian-Oldak, T. Diekwisch, D.M. Lyaruu, P. Bringas, H. C. Slavkin, Evidence for amelogenin nanospheres as functional components of secretory-stage enamel matrix, J. Struct. Biol. 115 (1995) 50–59, https://doi.org/10.1006/jsbi.1995.1029.
[52] A.G. Fincham, J. Moradian-Oldak, J.P. Simmer, P.E. Sarte, E.C. Lau, T. Diekwisch, H.C. Slavkin, Self-assembly of a recombinant amelogenin protein generates supramolecular structures, J. Struct. Biol. 112 (1994) 103–109, https://doi.org/10.1006/jsbi.1994.1011.
[53] E. Beniash, J.P. Simmer, H.C. Margolis, Structural changes in amelogenin upon self-assembly and mineral interactions, J. Dent. Res. 91 (2012) 967–972, https://doi.org/10.1177/0022034512457371.
[54] J. Zhang, J. Wang, C. Ma, J. Lu, Hydroxyapatite formation coexists with amyloid-like self-assembly of human amelogenin, Int. J. Mol. Sci. 21 (2020), https://doi.org/10.3390/ijms21082946.
[55] Z.S. Yuwei Fan, Rizhi Wang, Christopher Abbott, Janet Moradian-Oldak, Enamel inspired nano-composite fabrication through amelogenin supramolecular assembly, Biomaterials 28 (2007) 3034–3042, https://doi.org/10.1016/j.biomaterials.2007.02.016.
[56] C.S. Young, S. Terada, J.P. Vacanti, M. Honda, J.D. Bartlett, P.C. Yelick, Tissue engineering of complex tooth structures on biodegradable polymer scaffolds, J. Dent. Res. 81 (2002) 695–700, https://doi.org/10.1177/154405910208101008.
[57] W.P. Xu, W. Zhang, R. Asrican, H.J. Kim, D.L. Kaplan, P.C. Yelick, Accurately shaped tooth bud cell-derived mineralized tissue formation on silk scaffolds, Tissue Eng. Part A 14 (2008) 549–557, https://doi.org/10.1089/tea.2007.0227.
[58] M.J. Honda, Y. Shinmura, Y. Shinohara, Enamel tissue engineering using subcultured enamel organ epithelial cells in combination with dental pulp cells, Cells Tissues Organs 189 (2009) 261–267, https://doi.org/10.1159/000151743.
[59] W. Zhang, B. Vazquez, D. Oreadi, P.C. Yelick, Decellularized tooth bud scaffolds for tooth regeneration, J. Dent. Res. 96 (2017) 516–523, https://doi.org/10.1177/0022034516689082.